energies

Article

A Frequency Support Approach for Hybrid Energy Systems Considering Energy Storage

Dahu Li [1], Hongyu Zhou [2,*], Yuan Chen [3], Yue Zhou [1], Yuze Rao [1] and Wei Yao [2]

[1] State Grid Hubei Electric Power Co., Ltd., Wuhan 430077, China; dahu_li@126.com (D.L.); zhouyue198588@126.com (Y.Z.); hustryz@163.com (Y.R.)
[2] School of Electrical and Electronic Engineering, Huazhong University of Science and Technology, Wuhan 430074, China; w.yao@hust.edu.cn
[3] China Hubei Emission Exchange, Wuhan 430070, China; yuan_chen2023@126.com
* Correspondence: hongyu_zhou@hust.edu.cn

Abstract: In hybrid energy systems, the intermittent and fluctuating nature of new energy sources poses major challenges for the regulation and control of power systems. To mitigate these challenges, energy storage devices have gained attention for their ability to rapidly charge and discharge. Collaborating with wind power (WP), energy storage (ES) can participate in the frequency control of regional power grids. This approach has garnered extensive interest from scholars worldwide. This paper proposes a two-region load frequency control model that accounts for thermal power, hydropower, ES, and WP. To address complex, nonlinear optimization problems, the dingo optimization algorithm (DOA) is employed to quickly obtain optimal power dispatching commands under different power disturbances. The DOA algorithm's effectiveness is verified through the simulation of the two-region model. Furthermore, to further validate the proposed method's optimization effect, the DOA algorithm's optimization results are compared with those of the genetic algorithm (GA) and proportion method (PROP). Simulation results show that the optimization effect of DOA is more significant than the other methods.

Keywords: hybrid energy system; energy storage; wind power; support frequency; dingo optimization algorithm

Citation: Li, D.; Zhou, H.; Chen, Y.; Zhou, Y.; Rao, Y.; Yao, W. A Frequency Support Approach for Hybrid Energy Systems Considering Energy Storage. *Energies* **2023**, *16*, 4252. https://doi.org/10.3390/en16104252

Academic Editors: Hongjie Jia, Tao Jiang, Yukun Hu, Gen Li and Xiandong Xu

Received: 19 April 2023
Revised: 14 May 2023
Accepted: 19 May 2023
Published: 22 May 2023

1. Introduction

The deterioration of the ecological environment and the consumption of traditional fossil energy have become increasingly serious, prompting scholars worldwide to advocate for the accelerated development of clean and pollution-free renewable energy to achieve sustainable energy development [1–3]. However, the continuous grid connection of renewable energy presents significant challenges and pressures to the operation and maintenance of power systems [4–8]. Consequently, energy storage (ES) technology has become a critical foundation in building a new power system that promotes green and low-carbon energy transformation [9,10]. The cumulative installed capacity of new ES in China exceeded 4 million kilowatts by the end of 2021 [11,12]. To improve the consumption capacity of renewable energy, it is essential to accelerate the large-scale application of ES technology. Pumped storage, the most mature large-scale ES mode, operates by using surplus electric energy to pump water during low-demand periods and subsequently release the water to generate hydroelectric power during peak-demand periods.

Nowadays, the increasing installed capacity of wind power (WP) has become a major driving force for optimizing energy structure and achieving low carbonization. However, due to the intermittency, unpredictability, and fluctuation of WP, the stability of the power system is greatly affected and even threatened [13]. Therefore, to improve the stability of power systems with a high proportion of renewable energy, ES technology is introduced to cooperate with WP, making full use of the fast charge–discharge characteristics of energy storage. In addition, ES can be charged during high power generation periods of wind and PV plants, reducing the amount of abandoned power, and discharged during low power generation periods, reducing the start-up of thermal power units and promoting the absorption of new energy [14]. Thus, ES systems have a broad prospect in participating in frequency and peak regulation of power grids. However, due to the imperfections of the current domestic frequency regulation market and the high cost of ES products, the coordinated control means of ES systems and wind turbines for participating in grid frequency support have become a key topic of current research.

Among them, the vast majority of the literature takes WP prediction as the tracking target to make up for the error between the actual active power of WP and the prediction curve, to meet the assessment standards. In reference [15], the method of optimization before evaluation is adopted to carry out the research, and the feasibility of ES to improve the accuracy rate and qualified rate of active power in wind farms is verified by numerical examples. In the early stage of the development of WP, the power system has the priority to fully accept WP, and it is reasonable to take the predicted power of WP as the tracking target. Common control strategies can be roughly divided into the current control strategy that only considers the current charge and discharge demand and the advance control strategy which considers the ES demand in the future period. The former can meet the tracking requirements when the ES capacity is sufficient; otherwise, the latter strategy should be considered.

The high charge–low discharge strategy is the earliest ES control strategy. Reference [16] applied the high charge–low discharge strategy to a certain capacity of ES and found that the tracking effect of the combined system under different active power series of WP was different, but the paper did not make a quantitative analysis of this phenomenon. According to the simulation calculation in reference [17], a better tracking effect can be achieved when the ES capacity reaches 15~25% of the wind farm capacity. The advance control strategy can be divided into a one-step forward control strategy, an advanced control strategy based on control coefficient optimization, and an advanced control strategy oriented by objective function. In reference [18], battery limit states are partitioned according to state of charge (SOC). If the SOC is in the forbidden zone, the ES does not participate in the tracking of the power generation target; otherwise, the state of the SOC after fully tracking the power generation target is calculated. In reference [19], five control coefficients were designed to establish the relationship between the charging and discharging power of energy storage, using the planned active power of WP and ES SOC. Using the short-term prediction information in the time window, a set of control coefficient values corresponding to the time window is obtained by the particle swarm optimization algorithm. For the fan rotor kinetic energy control, reference [20] points out that the variable speed fan's participation in frequency modulation is generally realized by adding a frequency control loop to the active power controller, and proper adjustment of the gain of the control loop can enhance the frequency modulation effect of inertia control and droop control. In reference [21], inertial control and droop control are combined, and on this basis, the influence of different power levels of WP on frequency control performance is studied. Electricians began to realize the importance of the inertial response of WP [22,23]. Reference [24] provides a frequency modulation control strategy for wind turbines considering power reference values, which effectively uses the inertia of wind turbines to assist in solving frequency problems in power systems. In addition, the combination of the intelligent optimization algorithm and control method is also an effective means to solve the collaborative control of the power grid with the participation of raw energy sources. Reference [25] proposes a model prediction controller based on transient search optimization to realize the dual optimization process of load frequency control (LFC) of the power grid, so as to improve the dynamic and transient performance of the power grid.

The frequency support of hybrid energy systems with ES is a complex non-linear optimization problem. In general, the actual engineering application usually adopts the power distribution according to the adjustable capacity ratio, climbing speed ranking, and other ways, which cannot meet the optimal control requirements of the system. On the other hand, although the traditional mathematical optimization methods (such as the interior point method [26]) are fast, they have poor global search ability and tend to fall into the local optimal solution. Therefore, it cannot be easily solved using traditional mathematical methods. In contrast, intelligent optimization algorithms such as the genetic algorithm (GA) [27,28] and particle swarm optimization (PSO) [29] are more flexible in application and have stronger global search ability, but their solving speed is slow, which cannot meet the requirements of the automatic generation control (AGC) online control of large-scale regional power grids. Therefore, in this paper, we propose the use of the dingo optimization algorithm (DOA) to solve the problem [30]. To verify the effectiveness of our proposed method, we introduce an extended model based on the two-region model for simulation verification.

The rest of this paper is arranged as follows: Section 2 introduces the two-area load control model considering thermal power, hydropower, ES, and WP. At the same time, the objective function of this paper is introduced. Section 3 describes the DOA used in this paper in detail. In Section 4, based on the two-area load control model, the optimization effect of DOA under different power disturbances is simulated and analyzed. Meanwhile, to further test the optimization effect of DOA, the optimization results of DOA are compared with those of the proportion method (PORP) and GA [31,32]. Section 5 summarizes the contributions made in this paper in detail and gives the outlooks of future research.

2. Cooperative Control of ES and WP

2.1. Control Framework

The LFC of a power system aims to maintain the frequency of the power system within a certain error range, which provides the matching load with the lowest cost [33]. To study the regional frequency control problem under the cooperative participation of WP and ES, this paper introduces an extended model based on the IEEE standard two-region model to carry out simulation experiments and analysis.

The model is based on the extended two-region LFC model (Figure 1). The model mainly includes two regions and each region includes two steps: controller and power optimization. The controller is a traditional proportional–integral–derivative (PID) controller, which takes the real-time collected frequency deviation and network line contact deviation as input and the regulated total power of the whole regional power grid as output. Power optimization refers to the optimization of power allocation instructions for each AGC unit. Through power optimization, the frequency modulation potential of ES and WP can be fully exploited, to adapt to power disturbance more actively.

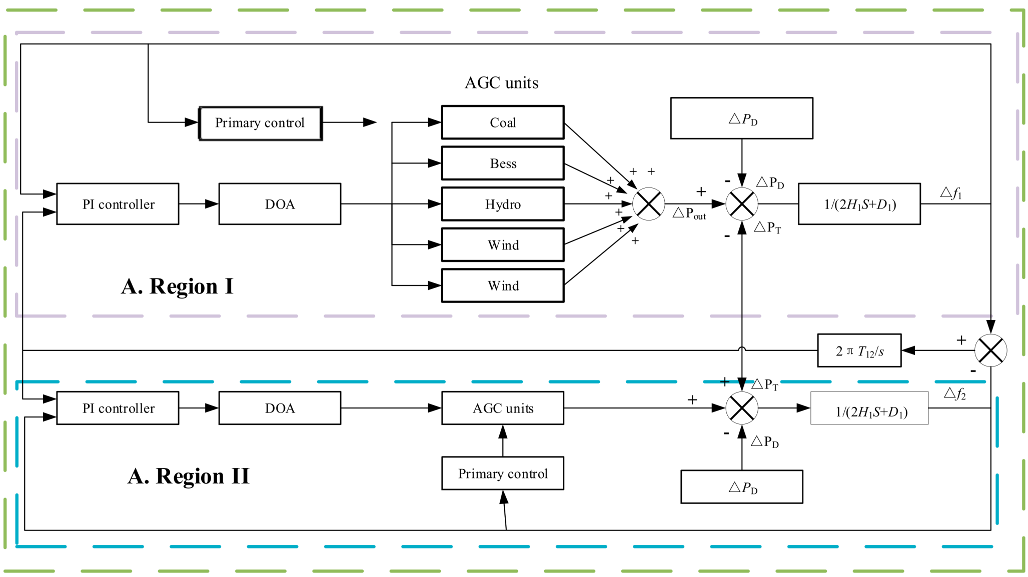

Figure 1. Two−region LFC model.

2.2. Dynamic Response Model

The frequency of the power grid is essentially an important index reflecting the quality and safety of power. The dynamic characteristics of frequency directly affect the start and stop of various control and protection devices in a power system. The appropriate dynamic response model of the unit is helpful to simulate the response process of the unit after receiving the adjustment command more accurately [34]. In addition to adjusting capacity, climbing rate, and frequency delay, the dynamic response model also has different energy transfer characteristics according to the unit type.

At present, the dynamic response process of AGC units is usually simulated by the frequency-domain model (Figure 2). T_d is expressed as the secondary frequency modulation delay, GRC is expressed as the generation ramp constraint, and $G(s)$ is expressed as the response transfer function, as shown in Table 1. The regulated output power can be written as

$$\Delta P_i^{\mathrm{out}}(t) = L^{-1}\left[\frac{G_i(s)}{s(1+T_\mathrm{d}^i s)} \cdot \sum_{k=1}^{N} \left[e^{-\Delta T\cdot(k-1)s} \cdot D_i^{\mathrm{in}}(k)\right]\right] \tag{1}$$

$$D_i^{\mathrm{in}}(k) = \Delta P_i^{\mathrm{in}}(k) - \Delta P_i^{\mathrm{in}}(k-1) \tag{2}$$

$$\Delta P_i^{\mathrm{out}}(k) = \Delta P_i^{\mathrm{out}}(t = k\cdot\Delta T) \tag{3}$$

where i is denoted as the ith unit. k is denoted as the kth control period. ΔP_i^{in} and $\Delta P_i^{\mathrm{out}}$ are represented as the command output and the actual output of the ith unit, respectively. ΔT is represented as the control period of the entire system, which is typically 1 to 15 s.

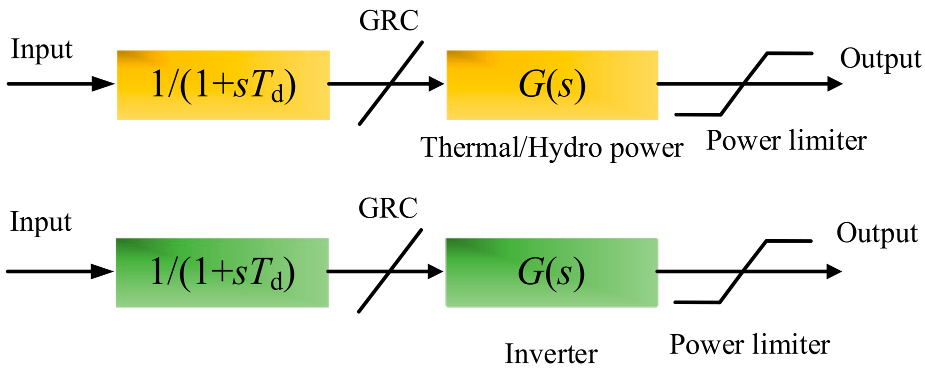

Figure 2. Dynamic response model.

Table 1. Dynamic response transfer function.

Type	Transfer Function
Thermal power	$\frac{1+T_1 s}{(1+T_2 s)(1+T_3 s)(1+T_4 s)}$
Hydropower	$\frac{(1-T_5 s)(1+T_6 s)}{(1+T_7 s)(1+T_8 s)}$
Wind power	$\frac{1}{1+T_9 s}$
Energy storage	$\frac{1}{1+T_{10} s}$

2.3. The Objective Function

In terms of the multi-type energy cooperative operation model constructed in this paper, the research direction of this paper is mainly to enhance the dynamic response regulation effect of power grids. Therefore, this paper takes minimizing the total deviation of the power response as the optimization objective, as shown below.

$$\min f = \sum_{j=k}^{N}\sum_{i=1}^{n}\left|\Delta P_i^{\mathrm{in}}(j) - \Delta P_i^{\mathrm{out}}(j)\right| \tag{4}$$

where N is represented as the number of periods, and n is expressed as the number of units.

Meanwhile, power balance constraints, capacity constraints, and energy transfer constraints are also considered.

Power balance constraint: in any control period, the total power of real-time regulation output should be equal to the sum of input instructions received by all frequency modulation units.

$$\sum_{i=1}^{n} \Delta P_i^{\text{in}}(k) - \Delta P_{\text{c}}(k) = 0 \tag{5}$$

where $\Delta P_i^{\text{in}}(k)$ is represented as the power output command received by the ith unit in the kth control cycle, and $\Delta P_{\text{c}}(k)$ is expressed as the real-time total regulation power in the kth control period.

Capacity constraints: the frequency range of each frequency modulation unit is different because of its different types.

$$\Delta P^{\text{in}}(k) \cdot \Delta P_i^{\text{in}}(k) \geq 0, \;\; i = 1, 2, \ldots, n \tag{6}$$

$$\Delta P_i^{\text{min}} \leq \Delta P_i^{\text{in}}(k) \leq \Delta P_i^{\text{max}} \;\; i = 1, 2, \ldots, n \tag{7}$$

where $\Delta P^{\text{in}}(k)$ is represented as the total power regulation command, and ΔP_i^{min} and ΔP_i^{max} are expressed as the minimum and maximum frequency modulation capacity, respectively.

3. DOA Algorithm

The DOA algorithm is a swarm intelligence optimization algorithm proposed by Peraza-Vazquez et al. in 2021 [35]. The DOA algorithm was inspired by the hunting behavior of the dog population. DOA designs three different search patterns associated with four rules. During the operation of the DOA algorithm, these search rules and patterns balance the exploitation and exploration of the solution space well. The DOA algorithm considers four aspects of the dingo population: group attack, persecution, scavenger, and survival rates. The mathematical model of the DOA algorithm is shown below.

The random initialization of the dingo population is shown in Equation (8). lb_i and ub_i denote the lower and upper bounds of individual $\vec{X}_i$, respectively. rand_i is represented as a random number between 0 and 1.

$$\vec{X}_i = \text{lb}_i + \text{rand}_i(\text{ub}_i - \text{lb}_i) \tag{8}$$

Group attack: Dingoes tend to move in groups when hunting large animals. The group behavior can be expressed by Equation (9).

$$\vec{X}_i(t+1) = \beta_1 \sum_{k=1}^{\text{na}} \frac{[\vec{\varphi_k}(t) - \vec{X}_i(t)]}{\text{na}} - \vec{X}_*(t) \tag{9}$$

where $\vec{X}_i(t+1)$ is represented as the next position of the dingo. na is represented as a random integer generated in the inverse order of [2, SizePop/2], where SizePop is represented as the size of the dingo population. $\vec{\varphi_k}(t)$ is the set of dingoes that engages in aggressive behavior, where $\varphi \subset \text{X}$, X is represented as a randomly generated population of dingoes. $\vec{X}_i(t)$ is represented as the current position of the dingo. $\vec{X}_*(t)$ is represented as the best dingo location found in the previous iteration. β_1 is a scaling factor used to change the trajectory of the dingo, usually taken as a uniformly generated random number between -2 and 2.

Persecution: Compared with hunting large animals, the behavior of a dingo hunting small animals can be expressed by Equation (10). $\vec{X}_i(t+1)$ is represented as the dingo's movement. $\vec{X}_i(t)$ is represented as the current position of the dingo. $\vec{X}_*(t)$ is represented as the best dingo location found in the previous iteration. β_2 is represented as a uniformly generated random number between 0 and 1. $\vec{X}_{r1}(t)$ is denoted as the position of $r1$ dingo chosen at random.

$$\vec{X}_i(t+1) = \vec{X}_*(t) + \beta_1 * e^{\beta_2} * (\vec{X}_{r1}(t) - \vec{X}_i(t)) \tag{10}$$

Scavenger: In addition, dingoes also have the behavior of looking for carrion in the process of random action, which can be expressed by (11).

$$\vec{X}_i(t+1) = \frac{1}{2}[e^{\beta_2} * \vec{X}_{r1}(t) - (-1)^{\sigma} * \vec{X}_i(t)] \tag{11}$$

where σ is represented as a binary number randomly generated by Figure 3a, $\sigma \in \{0, 1\}$.

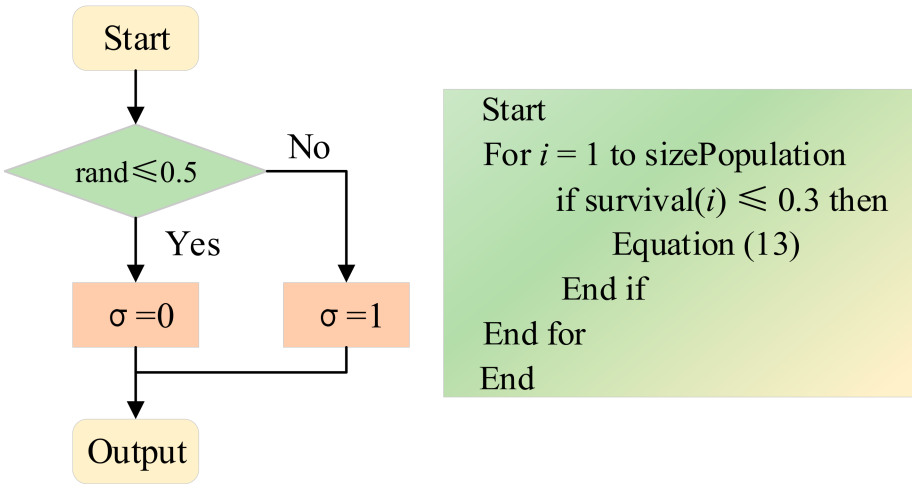

(**a**) (**b**)

Figure 3. σ value and survival process. (**a**) σ value; (**b**) survival process.

Survival rates: During the operation of the DOA algorithm, the survival rate is expressed by Equation (12).

$$\text{survival}(i) = \frac{\text{fitness}_{\text{max}} - \text{fitness}(i)}{\text{fitness}_{\text{max}} - \text{fitness}_{\text{min}}} \tag{12}$$

where $\text{fitness}_{\text{max}}$ and $\text{fitness}_{\text{min}}$ are represented as the worst and best fitness values, respectively. $\text{fitness}(i)$ is represented as the current fitness value. In addition, Equation (13) is applied to the case of low survival rate through Figure 3b.

$$\vec{X}_i(t) = \vec{X}_*(t) + \frac{1}{2}[\vec{X}_{r1}(t) - (-1)^{\sigma} * \vec{X}_{r2}(t)] \tag{13}$$

where $\vec{X}_i(t)$ is denoted as a dingo with a low survival rate that will be updated. $r1$ and $r2$ are represented as random numbers from 1 to population size. The overall operation flow of the DOA algorithm is shown in Figure 4.

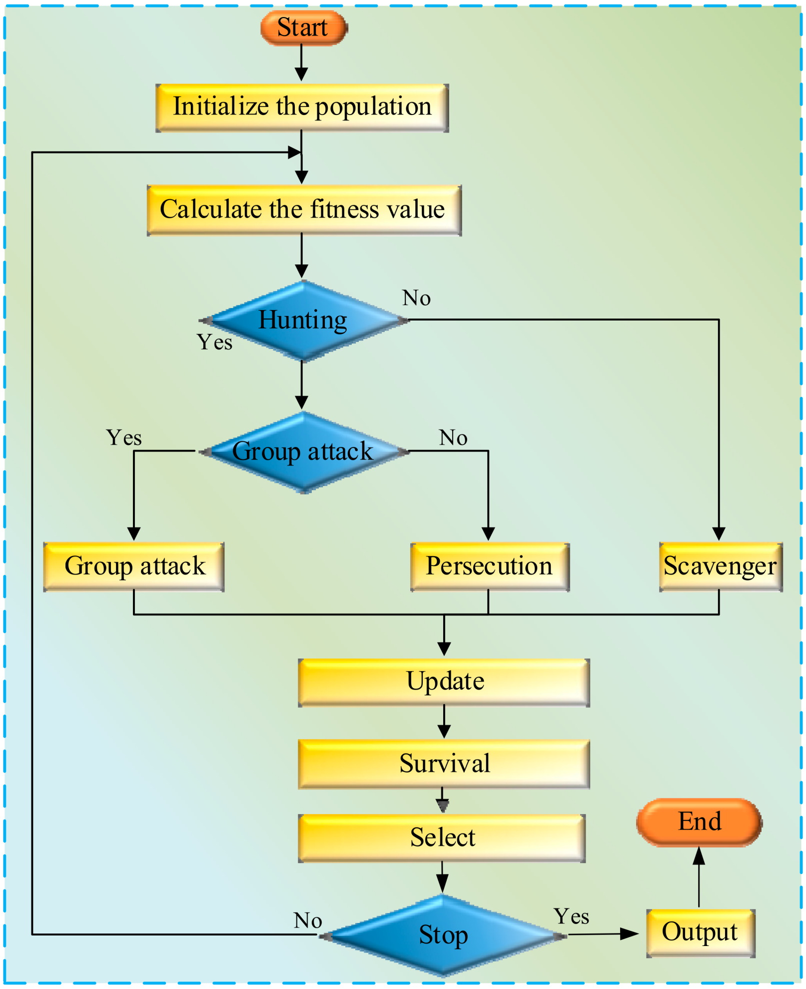

Figure 4. Flowchart of DOA.

4. Case Study

To test the online optimization effect of the proposed method, the effectiveness of the DOA algorithm is simulated and analyzed through the extended model of the IEEE standard two-area load control model, as shown in Figure 5a,b. Meanwhile, considering the current trend of energy structure transformation, this paper adjusts a single AGC unit to five different types of units, including one thermal power unit, one hydropower unit, two WP units, and one ES unit, as shown in Figure 5c. Considering the characteristics of thermal power, hydropower, WP, and ES in the actual project, we have limited the frequency regulation range and time delay, and the specific parameters are shown in Tables 2 and 3 [36,37]. All experiments in this paper were carried out on the MATLAB2020b platform. In addition, the PROP method and GA algorithm are adopted in this section to conduct comparative experiments, in which the populations of the GA algorithm and DOA algorithm are 50 and the iteration times of the algorithms are 30.

Table 2. Parameters of transfer functions [36,37].

Type	Parameter
Thermal power	$T_1 = 5$, $T_2 = 0.08$, $T_3 = 10$, $T_4 = 0.3$
Hydropower	$T_5 = 1$, $T_6 = 5$, $T_7 = 0.5$, $T_8 = 0.513$
Wind power	$T_9 = 0.01$
Energy storage	$T_{10} = 2$

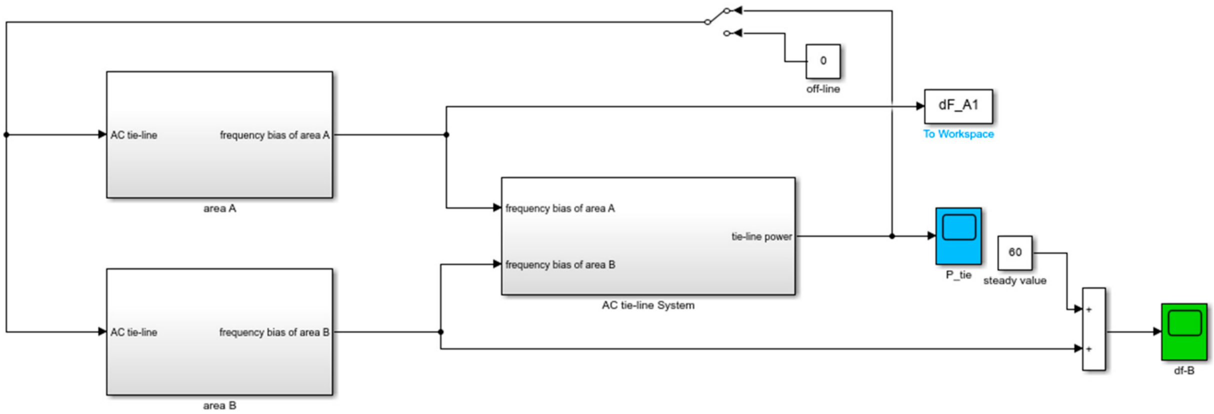

(**a**)

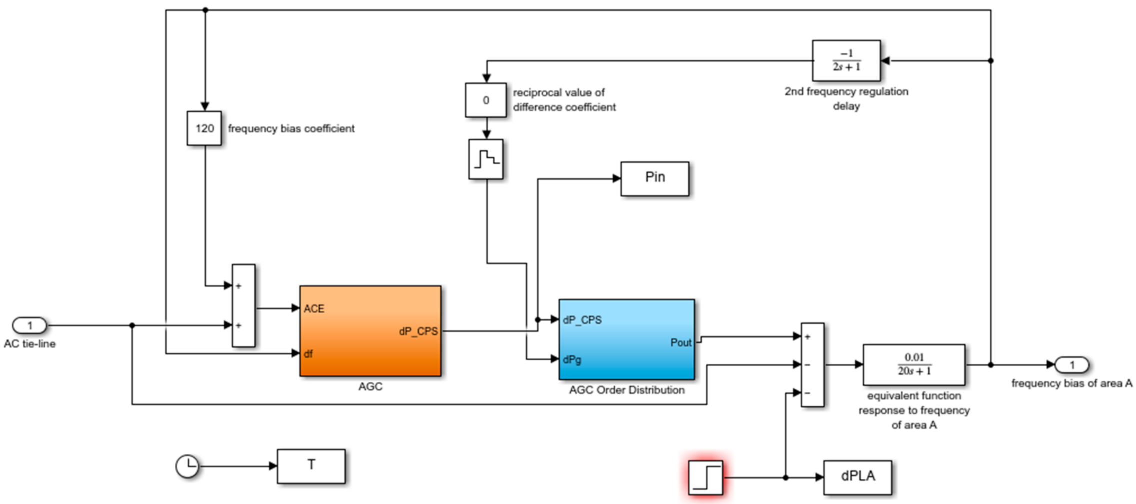

(**b**)

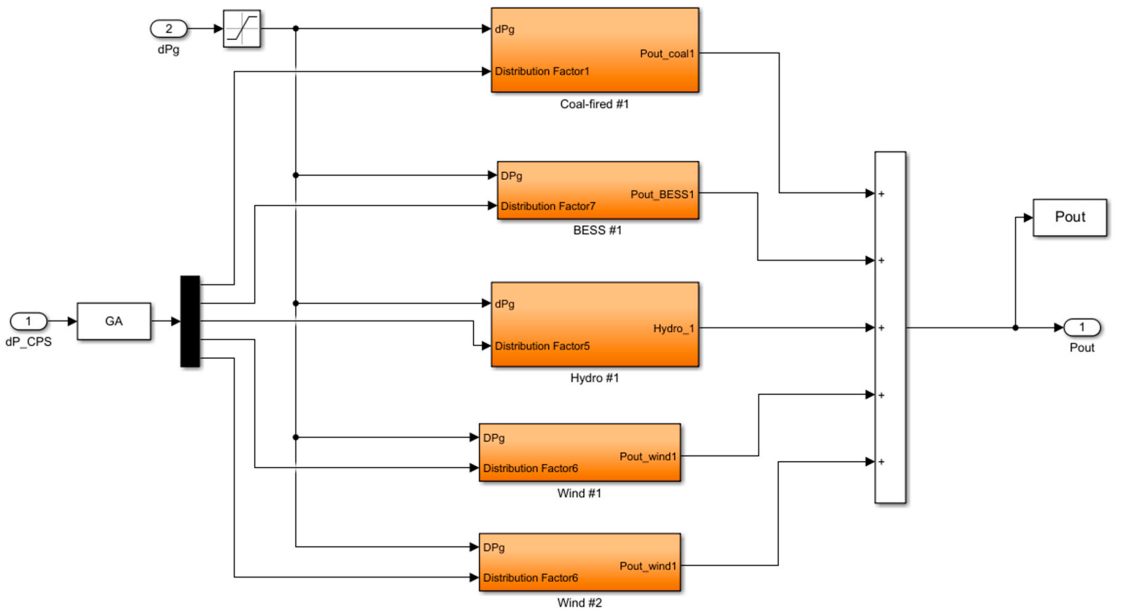

(**c**)

Figure 5. The extended model of IEEE standard two-area load control model. (**a**) Standard two-area load control model; (**b**) Area A; (**c**) AGC order distribution.

Table 3. Main parameters [36,37].

Type	T_d	ΔP^{rate}	ΔP^{max} (MW)	ΔP^{min} (MW)
Thermal power	60 s	30 MW/min	50	−50
Hydropower	5 s	150 MW/min	20	−10
Wind power	1 s	-	15	−5
Energy storage	1 s	-	8	−12

4.1. Power Disturbance $\Delta P_D = 50$ MW

The PROP method is used to allocate frequency regulation instructions proportionally according to the frequency regulation capacity of each frequency regulation unit. At present, the PROP method is widely used. However, it is difficult for the PROP method to take full advantage of the fast response speed of renewable energy units. Therefore, this paper adopts an intelligent optimization algorithm to improve the response speed of regional power grid frequency regulation and reduce power deviation. To verify the effectiveness of the DOA algorithm in the optimization of power network frequency modulation instruction, this section conducts a simulation experiment with power disturbance $\Delta P_D = 50$ MW. At the same time, the PROP method was added for comparison. The optimization effects of the two methods are shown in Figure 6. According to Figure 6, conclusions can be obtained as follows.

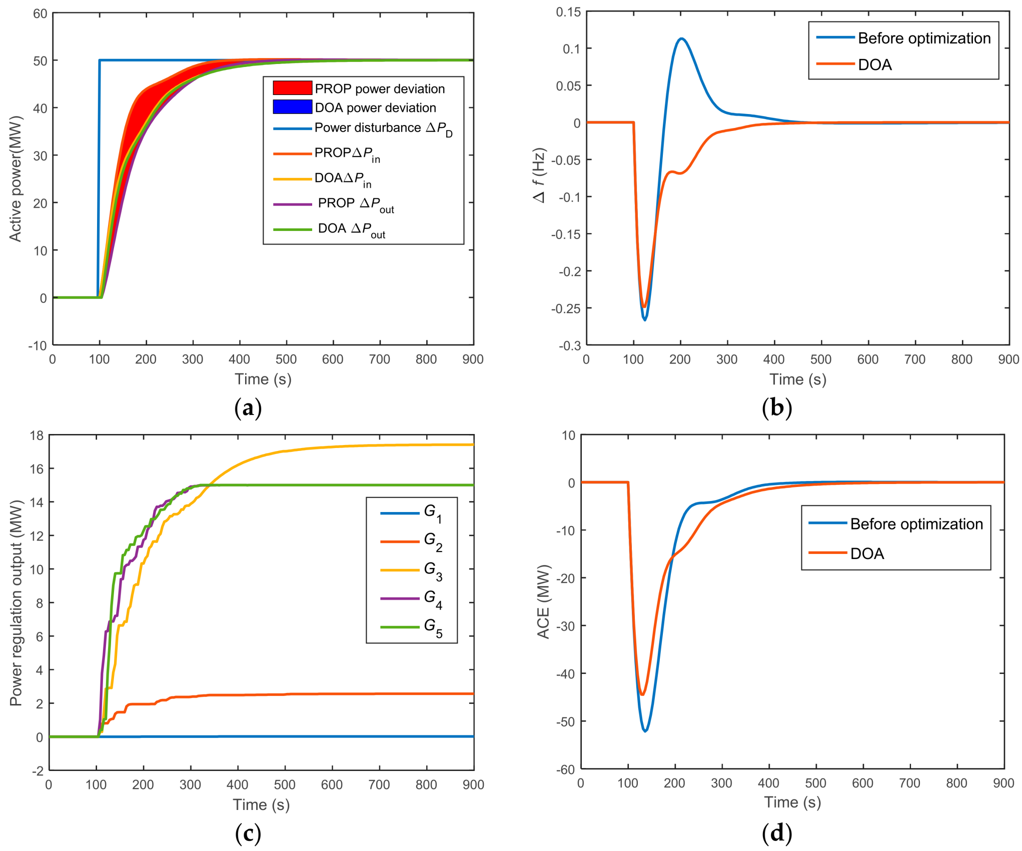

Figure 6. Adjusted results of DOA algorithm and PROP method (ΔP_D = 50 MW). (**a**) Regulation curve; (**b**) mean frequency deviation; (**c**) power regulation output under DOA algorithm; (**d**) area control error curve.

The overall power regulation curves of the PROP and DOA methods are shown in Figure 6a. The red area in the figure represents the power deviation of the PROP method, and the blue area represents the power deviation of the DOA method. The optimized DOA greatly reduces the total power deviation. Meanwhile, in the early stage of power regulation, the DOA algorithm can make full use of the characteristics of the fast regulation speed of renewable energy, and the power deviation in the early stage is greatly reduced. In addition, the power output curve and power instruction curve optimized by the DOA algorithm have a higher degree of fitting.

The mean frequency deviation curves of the PROP and DOA methods are shown in Figure 6b. The maximum deviation of the mean deviation curve after optimization of DOA algorithm is smaller than that of the PROP method. Meanwhile, the mean frequency deviation curve after optimization of the DOA algorithm rises more smoothly.

After DOA online optimization, the real-time power output curve of each frequency regulation unit is as shown in Figure 6c. Thermal power units did not participate in this frequency regulation, and the response speed of hydropower, WP, and ES is faster. Therefore, the characteristics of maximizing the utilization of WP and ES through algorithm optimization will contribute to the frequency stability of the regional power grid.

Area control error (ACE) is the deviation value formed by the load, generation power, frequency, and other factors in the control area. ACE reflects the balance between power generation and the load in the area. Compared with the PROP method, after the optimization of the DOA algorithm, the value of the lowest point of ACE increases. Meanwhile, the ACE curve optimized by the DOA algorithm rises more gently, as shown in Figure 6d.

In this case, to further test the online optimization performance of the DOA algorithm, the GA algorithm is added in this paper for comparison, as shown in Table 4. The three methods were evaluated in terms of $|\Delta f|$, accuracy, and power error. From Table 4, compared with the traditional PROP method, the intelligent optimization algorithm can dramatically improve the dynamic response performance of the AGC system of the regional power grid and significantly reduce the total power deviation. Meanwhile, compared with the GA algorithm, the DOA algorithm has better performance in the two evaluation indexes of the accuracy and power error, and the overall performance is better. Therefore, the simulation results show that the DOA algorithm is more suitable to deal with the frequency regulation optimization of the area power grid.

Table 4. The result of algorithm optimization.

ΔP_D (MW)	Algorithm	$\|\Delta f\|$	Accuracy	Power Error
50	PROP	0.0224 Hz	83.40%	369.2434 MW
	GA	0.0192 Hz	88.25%	10.8195 MW
	DOA	0.0192 Hz	88.36%	2.2626 MW

4.2. Power Disturbance $\Delta P_D = 70$ MW

When the power disturbance value is small, the thermal power frequency regulation units under the intelligent optimization algorithm almost do not participate in the frequency modulation process. Therefore, to verify the universality of the DOA algorithm in the optimization of power network frequency modulation instruction, this section conducts a simulation experiment with power disturbance $\Delta P_D = 70$ MW. Meanwhile, the PROP method was added for comparison. The optimization effects of the two methods are shown in Figure 7. From this, conclusions can be obtained as follows.

The overall power regulation curves of the PROP and DOA methods are shown in Figure 7a. The optimized DOA algorithm greatly reduces the total power deviation. Meanwhile, in the early stage of power regulation, DOA algorithms can take full advantage of the fast regulation of renewable energy sources, and the power deviation in the early stage is greatly reduced. In addition, in about 250 s, when the thermal power unit starts to undertake the task of frequency regulation, due to the slow response speed of the thermal power unit, Figure 7a shows that there is a significant deviation between the actual power output curve and the command power output curve.

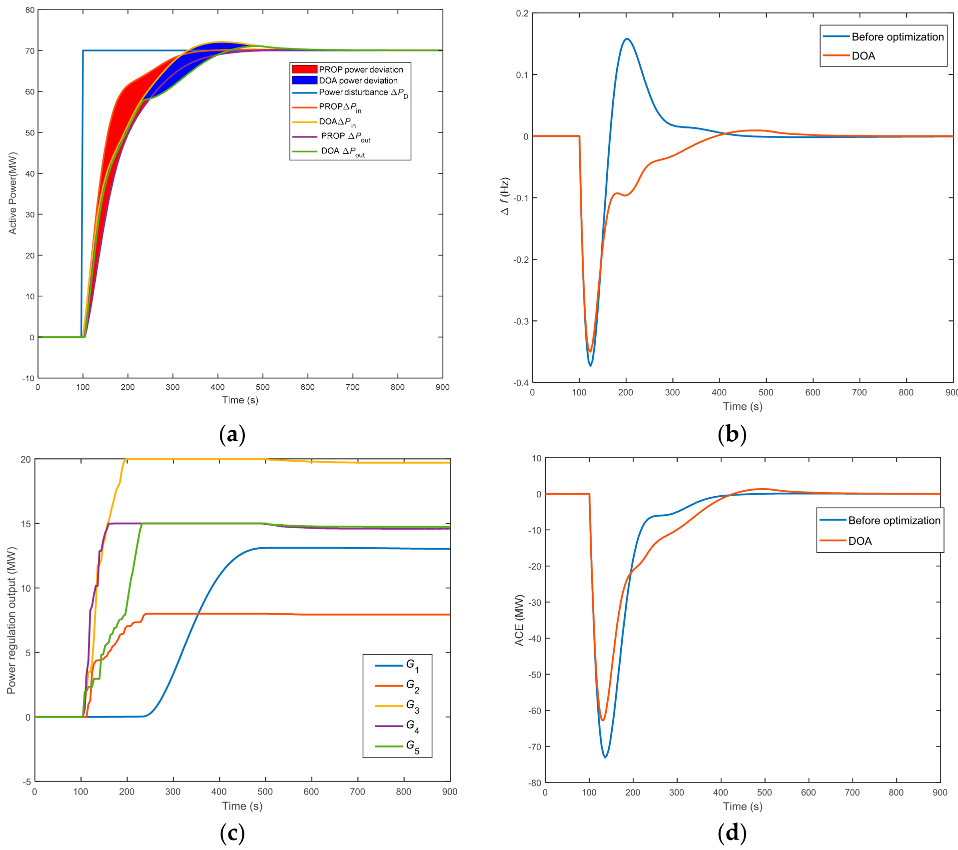

Figure 7. Adjusted results of DOA algorithm and PROP method (ΔP_D = 70 MW). (**a**) Regulation curve; (**b**) mean frequency deviation; (**c**) power regulation output under DOA algorithm; (**d**) area control error curve.

The mean frequency deviation curves of the PROP and DOA methods are shown in Figure 7b. The maximum deviation of the mean deviation curve after optimization of the DOA algorithm is smaller than that of the PROP method. Meanwhile, the mean frequency deviation curve after optimization of the DOA algorithm rises more smoothly.

After DOA online optimization, the real-time power output curve of each frequency regulation unit is as shown in Figure 7c. The response speed of thermal power units is relatively slow, while the response speed of hydropower, WP, and ES is faster. Therefore, the characteristics of maximizing the utilization of ES through algorithm optimization will contribute to the frequency stability.

Compared with the PROP method, after the optimization of the DOA algorithm, the value of the lowest point of ACE increases. Meanwhile, the ACE curve optimized by the DOA algorithm rises more gently.

In this case, to further test the online optimization performance of the DOA algorithm, the GA algorithm is added in this paper for comparison, as shown in Table 5. The three methods were evaluated in terms of $|\Delta f|$, accuracy, and power error. Compared with the GA algorithm, the DOA algorithm has better performance in the three evaluation indexes of the $|\Delta f|$, accuracy, and power error, and the overall performance is better. Therefore, the DOA algorithm is more suitable to deal with the frequency regulation optimization.

Table 5. The result of algorithm optimization.

ΔP_D (MW)	Algorithm	$\lvert\Delta f\rvert$	Accuracy	Power Error
70	PROP	0.0313 Hz	83.40%	516.94 MW
	GA	0.0302 Hz	86.87%	214.92 MW
	DOA	0.0296 Hz	87.02%	212.40 MW

4.3. Power Disturbance $\Delta P_D = -30$ MW

To further prove the effectiveness of the DOA algorithm, the simulation experiment when the step power disturbance is negative is added to this case. In this case, the step power disturbance is $\Delta P_D = -30$ MW. Meanwhile, this paper compares the optimization results of the DOA algorithm with the PROP method, as shown in Figure 8. According to Figure 8, it can be analyzed as follows.

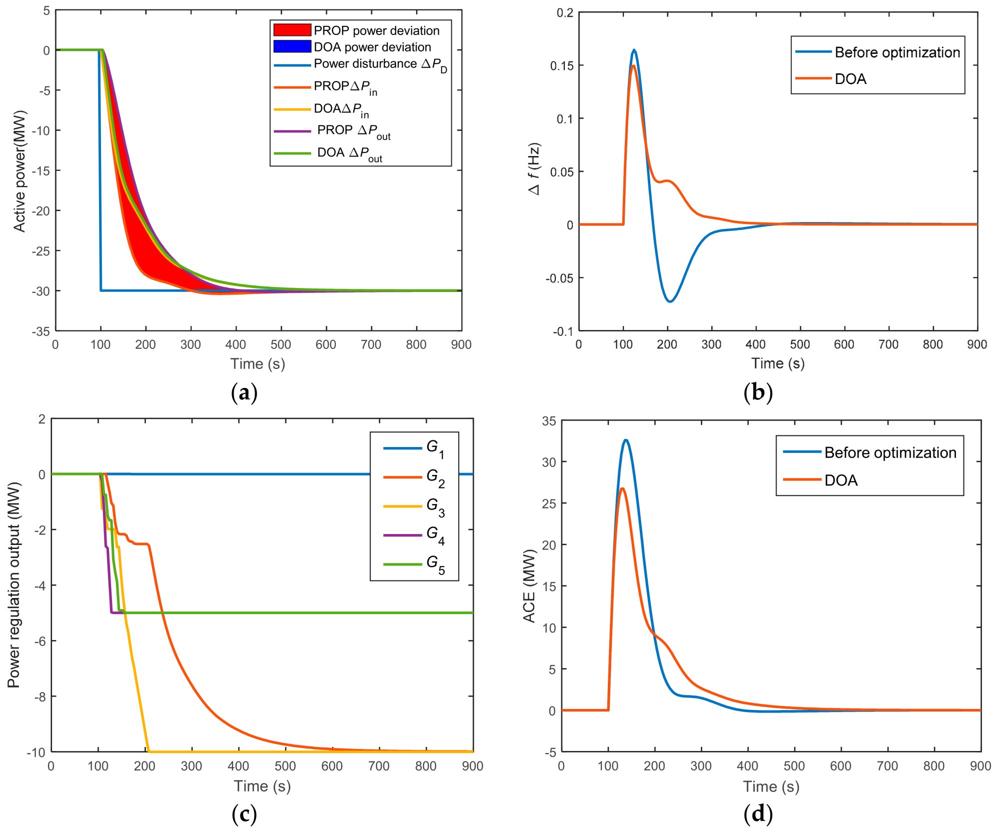

Figure 8. Adjusted results of DOA algorithm and PROP method ($\Delta P_D = -30$ MW). (**a**) Regulation curve; (**b**) mean frequency deviation; (**c**) power regulation output under DOA algorithm; (**d**) area control error curve.

From Figure 8a, when the power disturbance is negative, the optimized DOA algorithm also greatly reduces the total power deviation. Meanwhile, in the early stage of power regulation, DOA algorithms can take full advantage of the fast regulation of renewable energy sources, and the power deviation in the early stage is greatly reduced. In addition, the power output curve and power instruction curve optimized by the DOA algorithm have a higher degree of fitting.

The mean frequency deviation curves of the PROP and DOA methods are shown in Figure 8b. According to the simulation results, it is obvious that the maximum deviation of the mean deviation curve after optimization of the DOA algorithm is smaller than that of the PROP method.

After online optimization of DOA, the real-time power output curve of each frequency regulation unit is as shown in Figure 8c. Thermal power units have not participated in the frequency regulation process, and the frequency regulation task can be completed through hydropower, WP, and energy storage.

Compared with PROP method, after optimization of the DOA algorithm, the highest point of the ACE curve drops. Meanwhile, the ACE curve optimized by the DOA algorithm declines more gently.

From Table 6, compared with the traditional PROP method and the GA, the DOA algorithm can significantly improve the performance of the AGC of the regional power grid, significantly reduce the total power deviation, and has better overall optimization performance.

Table 6. The result of algorithm optimization.

ΔP_D (MW)	Algorithm	$\lvert\Delta f\rvert$	Accuracy	Power Error
−30	PROP	0.0144 Hz	81.94%	293.9385 MW
	GA	0.0115 Hz	87.90%	23.7335 MW
	DOA	0.0115 Hz	88.35%	3.5059 MW

4.4. Power Disturbance $\Delta P_D = -50$ MW

When the power disturbance ratio is small, thermal power units hardly participate in the frequency modulation work. This section adds that the step power disturbance is $\Delta P_D = -50$ MW in the simulation experiment. Meanwhile, the results of the DOA algorithm and PROP method are compared in Figure 9.

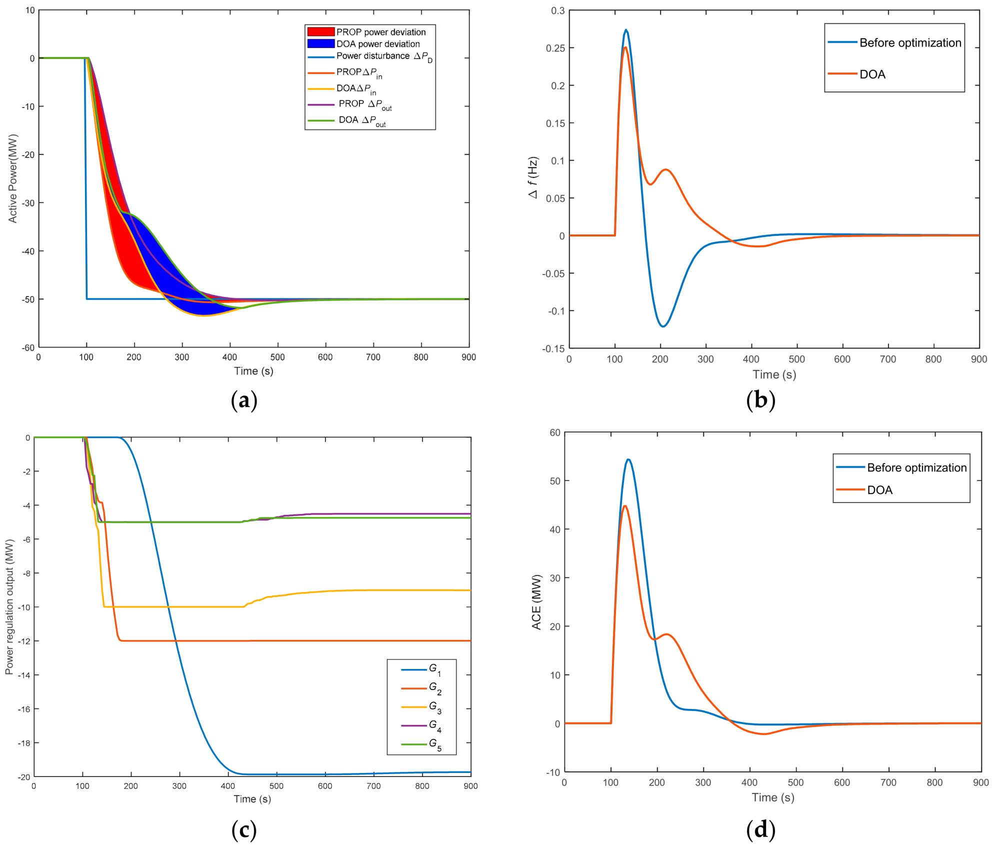

Figure 9. Adjusted results of DOA algorithm and PROP method (ΔP_D = −50 MW). (**a**) Regulation curve; (**b**) mean frequency deviation; (**c**) power regulation output under DOA algorithm; (**d**) area control error curve.

The overall power regulation curves of the PROP and DOA methods are shown in Figure 9a. When the power disturbance is negative, the optimized DOA algorithm also greatly reduces the total power deviation. Meanwhile, in the early stage of power regulation, the DOA algorithm can make full use of the characteristics of the fast regulation speed of renewable energy, and the power deviation in the early stage is greatly reduced.

The mean frequency deviation curves of the PROP and DOA methods are shown in Figure 9b. The maximum deviation of the mean deviation curve after optimization of the DOA algorithm is smaller than that of PROP.

After DOA online optimization, the real-time power output curve of each frequency regulation unit is as shown in Figure 9c. The response speed of thermal power units is relatively slow, while the response speed of hydropower, WP, and ES is faster. Therefore, the characteristics of maximizing the utilization of ES through algorithm optimization will contribute to the frequency stability.

Compared with the PROP method, after optimization of the DOA algorithm, the highest point of the ACE curve drops. Meanwhile, the ACE curve optimized by the DOA algorithm declines more gently, as shown in Figure 9d.

In this case, to further test the online optimization performance of the DOA algorithm, the GA algorithm is added in this paper for comparison. From Table 7, compared with the traditional PROP method, the intelligent optimization algorithm can significantly improve the performance of the AGC of the regional power grid and significantly reduce the total power deviation. Meanwhile, compared with the GA algorithm, the DOA algorithm has better performance in the two evaluation indexes of accuracy and power error, and the overall performance is better. Therefore, the DOA algorithm is more suitable to deal with frequency regulation optimization.

Table 7. The result of algorithm optimization.

ΔP_D (MW)	Algorithm	$\lvert\Delta f\rvert$	Accuracy	Power Error
−50	PROP	0.0240 Hz	81.94%	489.90 MW
	GA	0.0233 Hz	85.24%	331.25 MW
	DOA	0.0234 Hz	85.38%	312.13 MW

5. Conclusions

This paper investigates the cooperative control of wind power (WP) and energy storage (ES) involved in the secondary frequency regulation of the grid for hybrid energy systems. A new multi-energy secondary frequency regulation cooperative control method is proposed. The contributions of this paper are as follows.

Considering the accelerated process of energy structure transformation, the construction of a new power system continues to advance under the background. This paper constructed a regional power grid automatic generation control (AGC) model with the participation of WP and ES to improve the system's rapid response performance.

A multi-type energy cooperative control method based on the dingo optimization algorithm (DOA) algorithm is proposed, which realizes real-time online optimization of frequency modulation instructions through the DOA algorithm and quickly obtains the regulation scheme with a fast response speed and good convergence effect, to significantly improve the cooperative regulation performance of the regional power grid.

According to the recent energy development trend, future research plans are as follows.

According to the actual situation, the type and quantity of frequency modulation units are increased, and the appropriate intelligent optimization algorithm is studied to realize the cooperative control of the regional power grid.

For the frequency analysis and control of large hybrid energy systems, we can take advantage of deep learning classification, dimension reduction clustering, and other obvious advantages to improve the existing frequency problem modeling methods and prediction and evaluation effects.

Author Contributions: D.L.: Conceptualization, Writing, and Editing, H.Z.: Writing—Original draft preparation, Investigation, Y.C.: Reviewing and Supervision, Y.Z.: Reviewing and Supervision, Y.R.: Conceptualization, Resources, and W.Y.: Writing—Reviewing and Supervision. All authors have read and agreed to the published version of the manuscript.

Funding: This work is supported by the Science and Technology Project of State Grid Hubei Electric Power Co., Ltd. (Research on Key Technologies of Operation and Control of Hubei New Power System for Multi UHVDC Feed in and New Energy Base Development, No. 52150521000W).

Data Availability Statement: The data presented in this study are available on request from the corresponding author. The data are not publicly available due to funder policy.

Conflicts of Interest: The authors declare no conflict of interest.

Nomenclature

Variable	
ΔP_{T}	tie line power deviation
Δf	real-time frequency deviation
ΔP_{D}	power disturbance
ΔP_{out}	actual power regulation output
ΔT	control period
T_{d}	secondary frequency modulation delay
$G(s)$	transfer function
ΔP_i^{in}	command output of *i*th unit
$\Delta P_i^{\mathrm{out}}$	actual output of *i*th unit
ΔP_{c}	the real-time total regulation power
$\Delta P_i^{\min}$	the minimum frequency modulation capacity
$\Delta P_i^{\max}$	the maximum frequency modulation capacity
ΔP^{rate}	frequency regulation rate
$\Delta P^{\max}$	forward maximum frequency modulation capacity
$\Delta P^{\min}$	negative maximum frequency modulation capacity
$\vec{X}_i$	position of the dingo
$\vec{\varphi}_k(t)$	the set of dingoes that engages in aggressive behavior
$\vec{X}_*$	the best dingo location found in the previous iteration
β_1	a scaling factor used to change the trajectory of the dingo
β_2	a uniformly generated random number between 0 and 1
σ	a binary number randomly generated

Abbreviations	
ACE	area control error
AGC	automatic generation control
DOA	dingo optimization algorithm
ES	energy storage
GA	genetic algorithm
GRC	generation ramp constraint
LFC	load frequency control
PID	Proportional–integral–derivative
PROP	proportion method
PSO	particle swarm optimization
PV	photovoltaic
SOC	state of charge
WP	wind power

Parameter	
N	number of periods
n	number of units
$r1$	random numbers from 1 to population size
$r2$	random numbers from 1 to population size

References

1. Shi, Z.T.; Yao, W.; Zeng, L.K.; Wen, J.F.; Fang, J.K.; Ai, X.M.; Wen, J.Y. Convolutional neural network-based power system transient stability assessment and instability mode prediction. *Appl. Energy* **2020**, *263*, 114586. [CrossRef]
2. Zhou, H.Y.; Yao, W.; Sun, K.Y.; Ai, X.M.; Wen, J.Y.; Cheng, S.J. Characteristic investigation and overvoltage suppression of MMC-HVDC integrated offshore wind farms under onshore valve-side SPG fault. *IEEE Trans. Power Syst.* **2023**. [CrossRef]
3. Kannan, N.; Vakeesan, D. Solar energy for future world: A review. *Renew. Sustain. Energy Rev.* **2016**, *62*, 1092–1105. [CrossRef]
4. Zhou, H.Y.; Yao, W.; Sun, K.Y.; Zhao, Y.F.; Ai, X.M.; Wen, J.Y. A multi-level coordinated DC overcurrent suppression scheme for symmetrical bipolar MMC-HVDC integrated offshore wind farms. *Int. J. Electr. Power Energy Syst.* **2023**, *147*, 108880. [CrossRef]
5. Peng, X.T.; Yao, W.; Yan, C.; Wen, J.Y.; Cheng, S.J. Two-stage variable proportion coefficient based frequency support of grid-connected DFIG-WTs. *IEEE Trans. Power Syst.* **2020**, *35*, 962–974. [CrossRef]
6. Fu, X.Q. Statistical machine learning model for capacitor planning considering uncertainties in photovoltaic power. *Prot. Control. Mod. Power Syst.* **2022**, *7*, 51–63. [CrossRef]
7. Zhou, H.Y.; Yao, W.; Ai, X.M.; Li, D.H.; Wen, J.Y.; Li, C.H. Comprehensive review of commutation failure in HVDC transmission systems. *Electr. Power Syst. Res.* **2022**, *205*, 107768. [CrossRef]
8. Taher, A.M.; Hasanien, H.M.; Ginidi, A.R.; Taha, A.T.M. Hierarchical Model Predictive Control for Performance Enhancement of Autonomous Microgrids. *Ain Shams Eng. J.* **2021**, *12*, 1867–1881. [CrossRef]
9. Taher, A.; Said, A.; Eliyan, T.; Hafez, A. Analysis and Mitigation of Ground Grid Lightning Potential Rise. *Trans. Electr. Electron. Mater.* **2020**, *21*, 305–314. [CrossRef]
10. Yang, B.; Liu, B.Q.; Zhou, H.Y.; Wang, J.B.; Wu, S.W.; Shu, H.C.; Ren, Y.X. A critical survey of technologies of large offshore wind farm integration: Summary, advances, and perspectives. *Prot. Control Mod. Power Syst.* **2022**, *7*, 17. [CrossRef]
11. Belhachat, F.; Larbes, C. PV array reconfiguration techniques for maximum power optimization under partial shading conditions: A review. *Sol. Energy* **2021**, *230*, 558–582. [CrossRef]
12. Zhou, H.Y.; Yao, W.; Ai, X.M.; Zhang, J.; Wen, J.Y.; Li, C.H. Coordinated power control of electrochemical energy storage for mitigating subsequent commutation failures of HVDC. *Int. J. Electr. Power Energy Syst.* **2022**, *134*, 107455. [CrossRef]
13. National Development and Reform Commission. *"14th Five-Year Plan" New Energy Storage Development Implementation Plan*; National Development and Reform Commission: Beijing, China, 2022.
14. Zhou, H.Y.; Yao, W.; Zhou, M.; Ai, X.M.; Wen, J.Y.; Cheng, S.J. Active energy control for enhancing AC fault ride-through capability of MMC-HVDC connected with offshore wind farms. *IEEE Trans. Power Syst.* **2023**, *38*, 2705–2718. [CrossRef]

15. Liu, W.; Liu, Y. Hierarchical model predictive control of wind farm with energy storage system for frequency regulation during black-start. *Int. J. Electr. Power Energy Syst.* **2020**, *119*, 105893. [CrossRef]
16. Jin, W.T.; Li, B.; Xie, Z.J. An analysis for the need of a battery energy storage system in tracking wind power schedule output. *Energy Storage Sci. Technol.* **2013**, *2*, 294–299.
17. Kou, P.; Gao, F.; Guan, X.H. Stochastic predictive control of battery energy storage for wind farm dispatching: Using probabilistic wind power forecasts. *Renew. Energy* **2015**, *80*, 286–300. [CrossRef]
18. Teleke, S.; Baran, M.E.; Bhattacharya, S.; Huang, A.Q. Rule-based control of battery energy storage for dispatching intermittent renewal. *IEEE Trans. Sustain. Energy* **2010**, *1*, 117–124. [CrossRef]
19. Chai, W.; Cao, Y.F.; Li, Z.; Cai, X. An optimal energy storage control scheme for wind power and energy storage system based on state forecast. *Autom. Electr. Power Syst.* **2015**, *2*, 13–20.
20. Yan, H.M.; Li, X.J.; Ma, X.F.; Hui, D. Wind power output schedule tracking control method of energy storage system based on ultra-short term wind power prediction. *Power Syst. Technol.* **2015**, *2*, 432–439.
21. Vidyanandan, K.V.; Senroy, N. Primary frequency regulation by deloaded wind turbines using variable droop. *IEEE Trans. Power Syst.* **2013**, *28*, 837–846. [CrossRef]
22. Anaya-Lara, O.; Hughes, F.M.; Jenkins, N.; Strbac, G. Contribution of DFIG-based wind farms to power system short-term frequency regulation. *IEE Proc. Gener. Transm. Distrib.* **2016**, *153*, 164–170. [CrossRef]
23. Díaz-González, F.; Hau, M.; Sumper, A.; Gomis-Bellmunt, O. Participation of wind power plants in system frequency control: Review of grid code requirements and control methods. *Renew. Sustain. Energy Rev.* **2014**, *34*, 551–564. [CrossRef]
24. Knap, V.; Chaudhary, S.K.; Stroe, D.I.; Swierczynski, M.; Craciun, B.I.; Teodorescu, R. Sizing of an energy storage system for grid inertial response and primary frequency reserve. *IEEE Trans. Power Syst.* **2016**, *31*, 3447–3456. [CrossRef]
25. Ullah, N.R.; Thiringer, T.; Karlsson, D. Temporary primary frequency control support by variable speed wind turbines-Potential and applications. *IEEE Trans. Power Syst.* **2008**, *23*, 601–612. [CrossRef]
26. ATaher, M.; Hasanien, H.M.; Aleem, S.H.E.A.; Tostado-V, M.; Casan, M.; Turky, R.A.; Jurado, F. Optimal model predictive control of energy storage devices for frequency stability of modern power systems. *J. Energy Storage* **2023**, *57*, 106310.
27. Jiang, P.; Liang, L. Reactive power optimization of hybrid AC/HVDC power system combining interior point algorithm and genetic algorithm. *High Volt. Eng.* **2015**, *41*, 724–729.
28. PYan; Zeng, S.M.; Li, T.C.; Lu, J.D.; Yang, S.B.; Hu, X.K.; Zhang, B. Optimal scheduling of virtual power plant participating in AGC based on improved quantum genetic algorithm on multi-time scale. *Power Syst. Clean Energy* **2023**, *39*, 23–32.
29. Taher, A.; Said, A.; Eliyan, T.; Hafez, A. Optimum Design of Substation Grounding Grid Based on Grid Balancing Parameters using Genetic Algorithm. In Proceedings of the 2018 Twentieth International Middle East Power Systems Conference (MEPCON), Cairo, Egypt, 18–20 December 2018. [CrossRef]
30. Li, C.; Qin, L.J. Sizing optimization for hybrid energy storage system independently participating in regulation market using improved particle swarm optimization. *Acta Energ. Sol. Sin.* **2023**, *44*, 426–434.
31. Bairwa, A.K.; Joshi, S.; Singh, D. Dingo Optimizer: A Nature-Inspired Metaheuristic Approach for Engineering Problems. *Math. Probl. Eng.* **2021**, *2021*, 2571863. [CrossRef]
32. Li, J.W.; Yu, T.; Zhu, H.X.; Li, F.S.; Lin, D.; Li, Z.H. Multi-Agent Deep Reinforcement Learning for Sectional AGC Dispatch. *IEEE Access* **2020**, *8*, 158067–158081. [CrossRef]
33. Yang, L.; Li, S.N.; Huang, W.; Zhang, D.; Ma, H.S.; Xu, S.D.; Yang, B.; Zhang, S.X. Optimal Coordinated Control of Multi-Source for AGC with Participation of Wind and Solar Energy. *Power Syst. Prot. Control* **2020**, *48*, 43–49.
34. Wu, Z.Q.; Zhang, W.; Li, F.; Du, C.Q. Load frequency control of power system based on cloud neural network adaptive inverse system. *Electr. Power Autom. Equip.* **2017**, *37*, 86–98.
35. Liang, K.; Peng, X.T.; Qin, S.Y.; Wang, J.R.; Zhang, Z.; Chen, R.J. Study on synergetic control strategy for optimizing frequency response of wind farm augmented with energy storage system. *Proc. CSEE* **2021**, *41*, 2628–2640.
36. Peraza-Vázquez, H.; Peña-Delgado, A.F.; Echavarr, G.; Morales-Cepeda, A.B.; Velasco-Álvarez, J.; Ruiz-Perez, F. A bio-inspired method for engineering design optimization inspired by dingoes hunting strategies. *Math. Probl. Eng.* **2021**, *2021*, 9107547. [CrossRef]
37. Zhang, X.S.; Yu, T.; Yang, B.; Wang, H.Z. Optimal Mileage Based AGC Dispatch of a GenCo. *IEEE Trans. Power Syst.* **2020**, *35*, 2516–2526. [CrossRef]